Mathematical Biosciences and Engineering

http://www.aimspress.com/journal/MBE

MBE, 17(2): 1147–1167.
DOI: 10.3934/mbe.2020060
Received: 29 June 2019
Accepted: 16 October 2019
Published: 15 November 2019

Research article

Modeling selective therapeutic hypothermia in case of acute ischemic stroke using a 1D hemodynamics model and a simplified brain geometry

Yannick Lutz[1]*, Rosa Daschner[1], Lorena Krames[1], Axel Loewe[1], Giorgio Cattaneo[2], Stephan Meckel[3] and Olaf Dössel[1]

[1] Institute of Biomedical Engineering, Karlsruhe Institute of Technology (KIT), Karlsruhe, Germany
[2] Adceris GmbH & Co KG, Pforzheim, Germany (now at University of Stuttgart, Stuttgart, Germany)
[3] Department of Neuroradiology, Medical Center – University of Freiburg, Faculty of Medicine, Freiburg, Germany

* **Correspondence:** Email: publications@ibt.kit.edu; Tel: +49 -721608-47184; Fax: +49-721608-42789.

Abstract: Therapeutic hypothermia (TH) is an approved neuroproctetive treatment to reduce neurological morbidity and mortality after hypoxic-ischemic damage related to cardiac arrest and neonatal asphyxia. Also in the treatment of acute ischemic stroke (AIS), which in Western countries still shows a very high mortality rate of about 25 %, selective mild TH by means of Targeted Temperature Management (TTM) could potentially decrease final infarct volume. In this respect, a novel intracarotid blood cooling catheter system has recently been developed, which allows for combined carotid blood cooling and mechanical thrombectomy (MT) and aims at selective mild TH in the affected ischemic brain (core and penumbra). Unfortunately, so far direct measurement and control of cooled cerebral temperature requires invasive or elaborate MRI-assisted measurements. Computational modeling provides unique opportunities to predict the resulting cerebral temperatures on the other hand. In this work, a simplified 3D brain model was generated and coupled with a 1D hemodynamics model to predict spatio-temporal cerebral temperature profiles using finite element modeling. Cerebral blood and tissue temperatures as well as the systemic temperature were analyzed for physiological conditions as well as for a middle cerebral artery (MCA) M1 occlusion. Furthermore, vessel recanalization and its effect on cerebral temperature was analyzed. The results show a significant influence of collateral flow on the cooling effect and are in accordance with experimental data in animals. Our model predicted a possible neuroprotective temperature decrease of 2.5 °C for the territory of MCA perfusion after 60 min of blood cooling, which underlines the potential of the new device and the use of TTM in case of AIS.

Keywords: acute ischemic stroke; targeted temperature management; therapeutic hypothermia; finite element modeling; collateral circulation

1. Instruction

In animal stroke models, therapeutic hypothermia (TH) (temperature of 35 °C or below) led to an overall reduction of the infarct core size of 44 % [1]. Moreover, selective and time-limited cooling, using intracarotid cold saline infusion in an early phase of vessel reperfusion demonstrated neuroprotective effect [2, 3]. For acute ischemic stroke (AIS), the clinical use of TH proved to be safe and feasible [4], while its therapeutic efficacy remains controversially discussed and is currently under investigation in clinical trials [5, 6]. In 2018, a prospective cohort study of 113 patients showed that short-duration intraarterial selective cooling infusion plus mechanical thrombectomy (MT) led to a significant reduction in final infarct volume [7].

The cooling of arterial blood in the common carotid artery (CCA) is supposed to be an efficient method to induce local cerebral TH, since brain tissue temperature is mainly affected by cerebral hemodynamics. Alternative systemic hypothermia by means of surface or venous blood cooling involves major disadvantages (limited and slow brain temperature reduction and systemic adverse effects) [8]. A novel intracarotid blood cooling sheath, which allows for a combination with MT could enable TTM (selective mild TH) of the core and penumbra using the cooling effect of cold blood flow via ipsilateral collaterals prior to recanalization and cold reperfusion after recanalization [9, 10].

Unfortunately, direct measurement of local cerebral temperatures, which is needed for control of cooling and to assess resulting temperatures, is not possible without additional harm to the patient or a time-consuming MRI-based measurement. The use of computer models provides the unique opportunity to predict resulting cerebral temperatures. In this work, we used a 1D hemodynamics model of a detailed cerebral arterial tree and coupled a simplified 3D geometry of the human head to calculate tempo-spatial cerebral, as well as mean systemic temperature profiles. Our model allows to predict the decrease in cerebral temperature induced by intracarotid blood cooling as accompanying therapy to the treatment of AIS. Furthermore, the model can be used to evaluate the impact of collateral circulation on resulting temperature and to evaluate optimal cooling strategies.

2. Materials and methods

Cerebral temperatures are mainly affected by brain perfusion rates and the temperature of the arterial blood. To consider the effect of changing cerebral perfusion, the first part of this section describes how a detailed model of cerebral hemodynamics was built. For the hemodynamics model, all equations were implemented into Simulink, MATLAB (R2019a, The MathWorks, Nattick, MA, USA). The second part of this chapter deals with the development of a simplified 3D brain geometry, while the temperature calculation and the model coupling are explained in the last part.

2.1. Cerebral hemodynamics modeling

For blood flow simulations, a 1D hemodynamics approach was chosen to allow for realistic real time simulations of the whole arterial tree. The used transmission-line-approach considers the vessel wall's elasticity and enables a realistic simulation of pulsatile flow and pressure curves for every discretized arterial segment. Our model is based on Avolio's multi-branched model of the human arterial system [11], which was adjusted and extended by Schwarz et al. with the circle of Willis [12, 13]. Despite the expansions by Schwarz et al., the existing model contained only the largest cerebral arteries

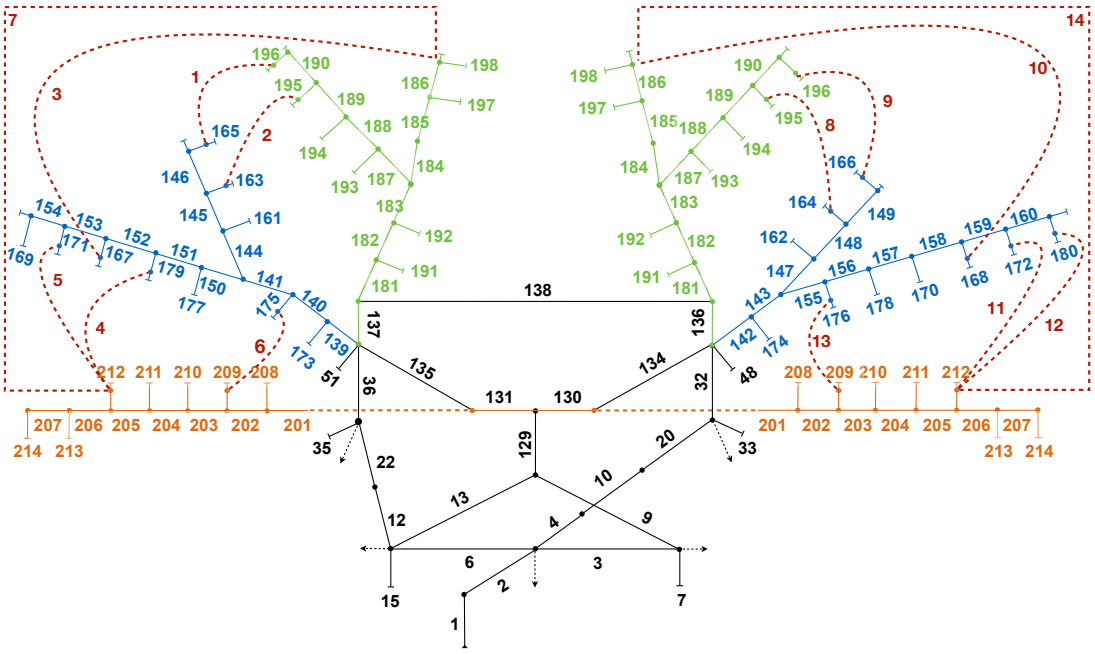

Figure 1. New hemodynamics model with detailed cerebral anatomy. The ACA is shown in green, the MCA in blue and the PCA in orange. The red dashed lines represent the integrated ipsilateral collaterals. The black dotted arrows indicate the branching of further arteries (aorta thoracica (torso), subclavia (arms), external carotid arteries), which have been omitted here for a clearer presentation. The numbers represent the respective arterial segments (compare Table 3).

(CA), which not further subdivided. Our goal was an individual modeling of the further course of the main CAs based on an extensive anatomical literature research. Since the anatomy of the CAs varies between individuals, we aimed to develop a model covering the major branching configuration ($\approx 64\,\%$ [14]) of the three main CAs (anterior, middle and posterior CA (ACA, MCA, PCA)). Therefore, we modeled a bifurcating MCA into superior and inferior M2 trunks and an ACA branching into a typical callosomarginal artery (CmA) and pericallosal arteries [14].

Overall, Avolio's model was expanded to establish 58 perfusion areas in the coupled 3D brain geometry. The cerebral structure of our resulting model is depicted in Figure 1. A more detailed description of the used transmission line approach and the extended model as well as a list of all determined parameters for modeling can be found in the Appendix (Section 5).

2.1.1. Terminal flow rates

The determination of individual mean terminal reference flow rates $\bar{q}_{\text{Term i}}$ for the physiological state is a requirement for the functionality of the hemodynamics model. For our model, we chose resistors as terminal segments - representing the capillary bed - and calculated their respective resistances using typical cerebral perfusion rates ($\nu_{\text{GM}}, \nu_{\text{WM}}$) of gray (GM) and white matter (WM):

$$q_{\text{Term i}} = \nu_{\text{WM}} \cdot V_{\text{Term i,WM}} + \nu_{\text{GM}} \cdot V_{\text{Term i,GM}}, \tag{2.1}$$

with $V_{\text{Term i}} = V_{\text{Term i,WM}} + V_{\text{Term i,GM}}$ being the volume perfused by the flow $q_{\text{Term i}}$ entering one

terminal segment i. To apply Eq. 2.1, perfusion rates of white and gray matter from Parkes et al. [15] were used. They took magnet resonance images and used arterial spin labeling to identify a relation between perfusion and patients sex and age. For our calculation, we considered a 60-year old man.

Since, to our knowledge, no information on the volume, shape or tissue type of individual terminal perfusion areas is available in the literature, a top-down approach was used to derive realistic values. As boundary flow conditions for the three main CA_j, we used flow rates q_{CA_j} proposed by Fahrig et al. [16], which are a compromise between afferent (internal cerebral artery, vertebral artery) and efferent (ACA, MCA, PCA) flow rates per hemisphere:

$$\text{ACA} : q_{CA_j} = \sum_i \bar{q}_{\text{Term i}} = 1.4\frac{ml}{s} \text{ with } i \in [1, 10], \tag{2.2}$$

$$\text{MCA} : q_{CA_j} = \sum_i \bar{q}_{\text{Term i}} = 2.6\frac{ml}{s} \text{ with } i \in [1, 12], \tag{2.3}$$

$$\text{PCA} : q_{CA_j} = \sum_i \bar{q}_{\text{Term i}} = 1.0\frac{ml}{s} \text{ with } i \in [1, 7]. \tag{2.4}$$

First of all, the total volumes of gray $V_{\text{total, GM}}$ and white tissue $V_{\text{total, WM}}$ of the entire brain were determined and a total brain volume V_{Br} of 1355 ml [17] was chosen. To determine the ratio between white and gray matter, data from Ge et al. [18] and Taki et al. [19] were used. The share of GM in the total brain volume $V_{\text{total, GM}}$ was set to 48 %, taking into account a division into cortex and subcortical GM. The proportion of WM was set to 35 %. The remaining 17 % were assigned to the brains' ventricles filled with cerebral spinal fluid (CSF). The volumes of GM and WM ($V_{\text{total, GM}}$,$V_{\text{total, WM}}$) were further subdivided into six areas V_{CA_j} belonging to one of the j main CA (ACA, MCA, PCA) for each hemisphere. For this purpose, results of Mut et al. [20] were used, which provide the contribution of CA_j to the total cerebral blood supply. Under consideration of the boundary flow conditions (compare Eq. 2.2-2.4), V_{CA_j} was divided into volumes of GM and WM:

$$V_{j,GM} = \frac{q_{CA_j} - V_{CA_j} \cdot \nu_{WM}}{\nu_{GM} - \nu_{WM}}, \tag{2.5}$$

$$V_{j,WM} = V_j - V_{j,GM}. \tag{2.6}$$

The location of each terminal perfusion area and individual composition of GM and WM were assessed from literature [20, 21, 22, 23]. In this context, we assumed that the volumes V_{CA_j} are divided evenly among all respective terminal perfusion areas. Figure 2b shows an exemplary perfusion area belonging to two terminal MCA segments. Following our approach, we obtained terminal perfusion areas consisting of either cortical GM only, subcortical GM only, or gray and WM.

2.1.2. MCA M1 occlusion

The aim of this work is the prediction of brain temperatures for the treatment of AIS with selective TH. To model resulting ischemic blood flow conditions, we considered a possible MCA M1 occlusion in the hemodynamics model. The first M1 artery segment (compare segment 139 in Figure 1) was subdivided into three parts. In the first part (proximal) and the third part (distal) the physiological artery

parameters were kept unchanged (compare Section 5). The second part reflects the actual occlusion and was set to have a length of 0.5 cm. It was implemented as a single resistor. Moreover, the occlusion degree S was set to 100 %, which leads to a completely occluded vessel:

$$r_{\text{Sten}} = r_0 \cdot (1 - \frac{S}{100\,\%}), \tag{2.7}$$

with r_0 being the initial M1 artery radius and r_{Sten} the radius of the occluded segment.

2.1.3. Collateral circulation

In addition to the blood supply through the main CA, there is a subsidiary supply of the brain regions through leptomeningeal collaterals. They can act as anastomotic channels in conditions where cerebral blood flow is pathologically altered and collateral flow through the circle of Willis is inadequate [24]. This collateral circulation is particularly important in case of an MCA stenosis or occlusion [25]. We used data of Vander Eecken and Adams [26] about the occurrence and dimensions of meningeal collaterals to include seven secondary ipsilateral collaterals between the main CA in both hemispheres (3 ACA-MCA, 3 MCA-PCA, 1 ACA-PCA).

2.2. Simplified brain geometry

The brain model (compare Figure 2a) consists of the cerebrum (including the ventricles), a surrounding layer representing the subarachnoid space (outer CSF space, r= 2.4 mm [27]), a layer for the dura mater (outermost cerebral membrane, r= 0.55 mm [28]), a layer for the skull (r= 5.36 mm [29]) and a layer for the skin (r= 3.46 mm, consisting of epidermis, hypodermis and reticular dermis [30, 31]). For the brain, an average length, width and depth of 17 cm, 11 cm and 13 cm was used and the total brain volume V_{Br} (including ventricles), as well as all calculated volumes (compare Section 2.1) were considered. Furthermore, the presence of an insula on both hemispheres was considered, as well as an even cortex thickness.

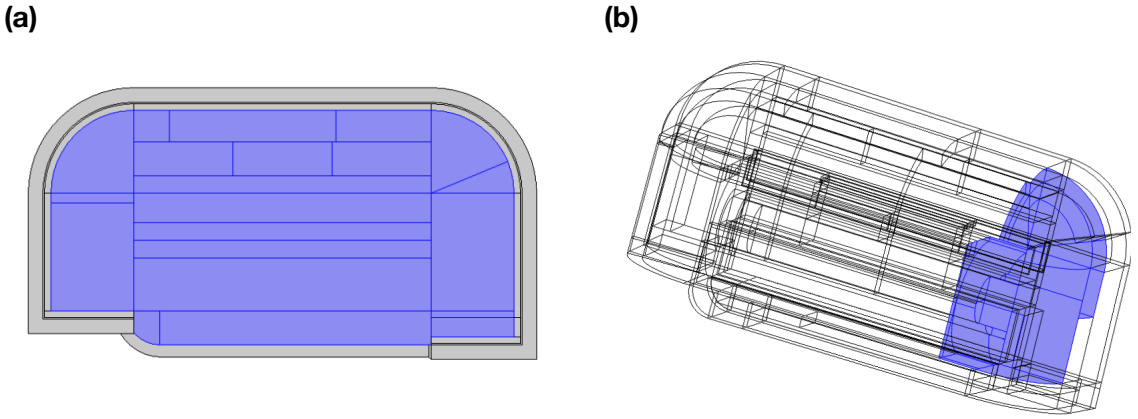

Figure 2. (a): Medial view of the right hemisphere of the used geometry for temperature calculation. The blue area represents the brain tissue. (b): Medial view of the perfusion area of two terminal MCA segments close to the arteries 167&179 (compare Section 5).

2.3. Temperature calculation

The calculation of cerebral temperatures was performed using the bioheat transfer module of COMSOL Multiphysics 5.4, which is based on Pennes' bioheat equation. The equation considers heat conduction in tissue, heat exchange between arterial blood and tissue and heat generation by metabolism to calculate spatial- and time-dependent temperature T in living tissue:

$$\rho_T c_T \frac{\partial T}{\partial t} = \nabla(\lambda_T \nabla T) - c_{Bl} \cdot \nu_{Bl} \cdot (T - T_a) + P_{\text{Met}} \tag{2.8}$$

In this equation, ρ_T is the density, c_T the specific heat and λ_T the thermal conductivity of the tissue. c_{Bl} is the specific heat of blood, ν_{Bl} the volumetric perfusion rate, T_a the arterial blood temperature and P_{Met} the metabolic heat [32]. Besides bioheat transfer, convection and radiation were considered in our simulations for all tissue being in contact with the environment. The ambient temperature was assumed to be 20 °C and the head to be an ideal black radiator ($\varepsilon = 1$). All other parameters used for temperature calculation can be found in Table 1. Parameters of regions consisting of a mixture of tissues were calculated as percentage-weighted sum of the individual tissue parameters considering the respective volume.

For every segment i out of all 58 perfusion segments in our 3D geometry, the spatial temperature was calculated as follows:

$$\rho_{\text{Term i}} \cdot c_{\text{Term i}} \frac{\partial T_{\text{Term i}}}{\partial t} = \nabla(\lambda_{\text{Term i}} \nabla T_{\text{Term i}}) - c_{Bl} \cdot \frac{q_{\text{Term i}}}{\text{V}_{\text{Term i}}} \cdot (T_{\text{Term i}} - T_a) + P_{\text{Met, Term i}} \tag{2.9}$$

Table 1. Tissue properties of the modeled tissue layers.

Tissue	ν $[\frac{1}{s}]$	P_{Met} $[\frac{W}{m^3}]$	λ $[\frac{W}{m \cdot K}]$	c $[\frac{J}{kg \cdot K}]$	ρ $[\frac{kg}{m^3}]$	Source
Epidermis	0	0	0.45	3680	1085	[33]
reticular dermis	0.0017	368	0.45	3680	1085	[33]
hypodermis	0.00029	300	0.21	2495	920	[33]
CSF	0	0	0.6	4150	1002	[33]
Dura mater	0.00072	0	0.6	1672	1370	[33]
Skull	0.00006	130	0.75	1700	1500	[33]
GM	0.009	16230.62	0.547	4095.5	1044.5	[33]
WM	0.0041	4497.71	0.481	3582.2	1041	[33]
Blood	0	0	0.517	3617	1049.75	[34]

2.3.1. Systemic temperature coupling

The geometry for cerebral temperature calculation consists of brain tissue and surrounding layers. The blood flowing through the brain circulates through the bloodstream of the remaining body, which affects the blood temperature before the cooling catheter and the systemic temperature T_{sys} of the remaining body itself. To model this influence, a mathematical model of the systemic body was taken into account. The model also uses Pennes' bioheat equation but without a term for heat diffusion and

heat generation by metabolism. Therefore, the systemic model only considers heat exchange between the systemic body and the blood coming from the brain:

$$M_{Sys}c_{Sys} \cdot \frac{dT_{Sys}}{dt} = \sum_i \rho_{Bl} \cdot c_{Bl} \cdot \bar{q}_{\text{Term i}} \cdot (T_{Sys} - T_{\text{Term i}}), \tag{2.10}$$

where T_{Sys} is the temperature of the whole remaining body and M_{Sys} is the respective mass, which was set to 75 kg. The factor $\bar{q}_{\text{Term i}}$ is the mean flow into the respective terminal segment i calculated by the blood flow simulation (compare Section 2.1) and $T_{\text{Term i}}$ is the mean temperature of the coupled perfusion area i. The systemic heat capacity c_{Sys} was set to 3470 $\frac{J}{kg \cdot K}$.

2.3.2. Blood cooling

As mentioned in the introduction, the developed model should predict the decrease in cerebral spatial temperature induced by intracarotid blood cooling as accompanying therapy to the treatment of AIS. Therefore, we considered a recently developed endovascular catheter system, which is placed in the CCA [9]. The catheter induces TH in the ischemic brain tissue using the cooling effect of cerebral blood flow via collaterals. For this purpose, intracarotid blood cooling by means of a cold saline closed loop is performed. In vitro experiments with artificial blood revealed a mean temperature drop between the catheter inlet and outlet of $-2.17 \pm 0.07\,^{\circ}\text{C}$ and $-1.55 \pm 0.06\,^{\circ}\text{C}$ for flow rates of 250 and 400 $\frac{ml}{min}$, respectively [9]. Therefore, we chose a temperature decrease $\Delta T_{Cooling}$ of 2.0 °C for our temperature calculations. This means, that the "cold blood" flowing into the right hemisphere via the internal cerebral artery was 2.0 °C colder than the systemic temperature T_{Sys} at each time point of the temperature calculation:

$$T_a = T_{\text{Sys}} - 2\,^{\circ}\text{C}. \tag{2.11}$$

2.3.3. Effect of cooling on flow and metabolism

In an extensive literature research, Konstas et al. [35] investigated the hypothermic effects on cerebral blood flow and metabolism. Evaluating data from animal and human studies, they concluded that blood flow and metabolism decrease exponentially over decreasing brain temperature, as long as cerebral temperatures stay above 25 °C. They derived the following equation:

$$\chi(T) = \chi_{37} \cdot 2.961^{0.08401 \cdot (T - 37^{\circ}C)}, \tag{2.12}$$

where χ_{37} is the baseline cerebral blood flow (in $\frac{\text{ml}}{\text{s}}$) or metabolic heat (in $\frac{\text{W}}{\text{m}^3}$) for 37 °C. In our model, we considered temperature dependent blood perfusion rates and metabolic heat generation for every individual perfusion area i:

$$\nu_{Term\,i}\,(T_{\text{Term i}}) = \frac{\bar{q}_{\text{Term i},37} \cdot 2.961^{0.08401 \cdot (T_{\text{Term i}} - 37\,^{\circ}C)}}{V_{\text{Term i}}}, \tag{2.13}$$

$$P_{\text{Met, Term i}}\,(T_{\text{Term i}}) = P_{\text{Met i},37} \cdot 2.961^{0.08401 \cdot (T_{\text{Term i}} - 37\,^{\circ}C)}. \tag{2.14}$$

2.3.4. Influence of collaterals

As already mentioned, collateral circulation plays a major role for remaining perfusion rates in case of AIS. Therefore, collateral blood flow has also crucial impact on the spatial and temporal cerebral temperature profiles. Additionally, different blood temperatures in the individually modeled collaterals affect the results. To consider this fact, a blood-temperature-mixing was realized:

$$T_{a,b} = \frac{T_a \cdot q_a + T_b \cdot q_b}{q_a + q_b}. \tag{2.15}$$

Here, $T_{a,b}$ describes the resulting temperature after the mixing of the fluxes q_a with temperature T_a and q_b with temperature T_b. This approach was used to consider the effect of flow mixing for blood coming from the anterior communicating artery (segment 138), the posterior communicating artery (segment 135&134) and for blood coming from the ipsilateral collaterals. However, we did not differentiate the blood temperatures for every collateral individually. For the influences of the collateral flows from the ACA to MCA, only the mean temperatures in the ACA and MCA perfusion areas ($T_{V_{\mathrm{ACA}}}$, $T_{V_{\mathrm{MCA}}}$) were considered. This procedure was also used for the collateral flows from PCA to MCA and PCA to ACA.

3. Results

3.1. Resulting blood flow

For the physiological state without an MCA M1 occlusion, the hemodynamics model yielded undiminished flow rates close to the predefined flow boundary conditions (compare Eq. 2.2-2.4). For the ACA, the sum of the mean flow into all terminal segments was 1.36 $\frac{\mathrm{ml}}{\mathrm{s}}$, for the MCA it was 2.57 $\frac{\mathrm{ml}}{\mathrm{s}}$ and for the PCA it was 0.98 $\frac{\mathrm{ml}}{\mathrm{s}}$. The ipsilateral collaterals were only weakly perfused ($\approx 0.00065 \frac{\mathrm{ml}}{\mathrm{s}}$). The resulting flow curves can be also seen as dashed lines in Figure 3.

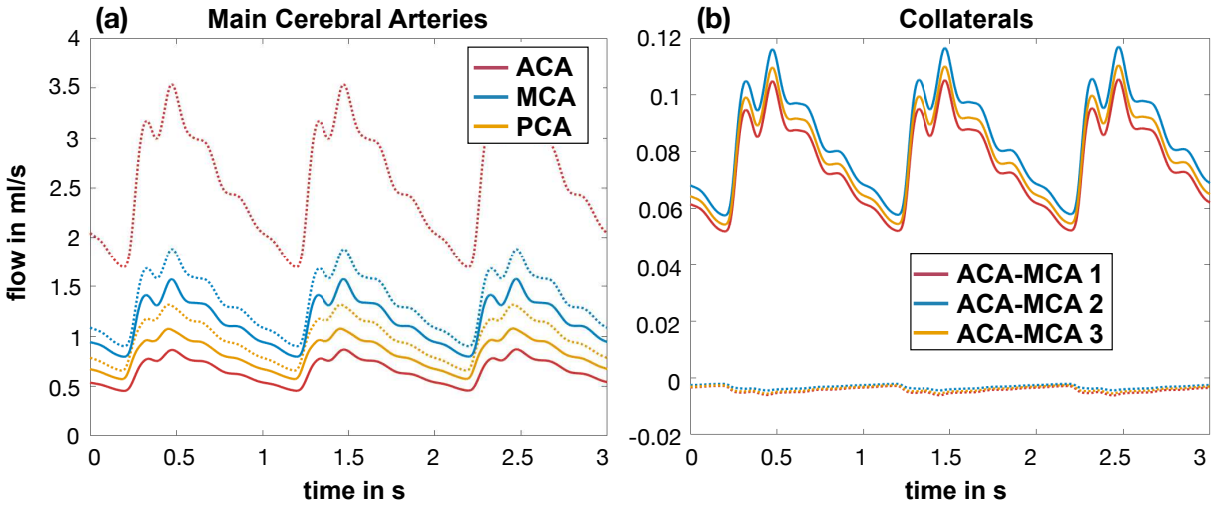

Figure 3. (a): Sum of flow in all terminal segments of the respective main cerebral artery in the right hemisphere. (b): Flow curves of the ACA-MCA collaterals in the right hemisphere. (The dashed lines represent the physiological case, while the solid lines represent the ischemic condition resulting from a 100 % MCA M1 occlusion.)

AIS was simulated considering a 100 % occlusion of the M1 segment of the right MCA (compare Section 2.1.2). Consequently, the summed mean flow into all terminal segments of the respective main CAs decreased (solid lines in Figure 3a). Compared to the physiological case, the flow for the ACA and PCA decreased by approximately 15 %, whereas the flow for the MCA decreased by 75 % ($\bar{q}_{\text{MCA, ischemic}} \approx 0.65\,\frac{\text{ml}}{\text{s}}$). Now, the ipsilateral collaterals were the only pathway left. The flow curves through the collaterals from the ACA to the MCA in the ischemic case are shown as solid lines in Fig 3a. A resulting summed mean flow of $0.241\,\frac{\text{ml}}{\text{s}}$ for the ACA-MCA collaterals and of $0.413\,\frac{\text{ml}}{\text{s}}$ for the PCA-MCA collaterals was predicted. The sum of the six individual fluxes was $0.65\,\frac{\text{ml}}{\text{s}}$, which corresponded to the remaining average flow through the MCA.

3.2. Resulting temperatures

In this section, the resulting cerebral temperatures are presented. For the calculation the resulting averaged flow rates of the hemodynamics model were used. In the first part, results are shown for continuous physiological and ischemic flow conditions. However, since the cooling catheter allows combined therapy by means of vessel recanalization with MT, an increase in perfusion after a successful MT is expected. For the purpose of modeling recanalization, the degree of occlusion was lowered (from $S = 100\,\%$ to $S = 0\,\%$) after 10 or 20 min of cooling. The results of this approach are presented in Section 3.2.2.

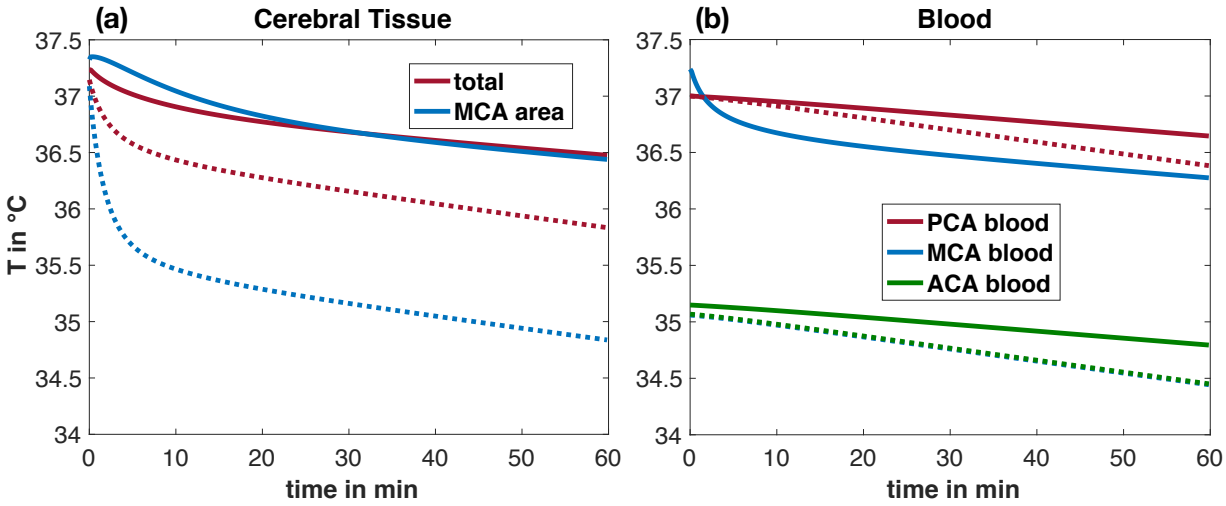

Figure 4. Course of cerebral tissue temperatures (a) and arterial blood temperatures (b) over time for selective intracarotid blood cooling. The ischemic case is shown using solid lines, while the dotted lines represent the physiological case.

3.2.1. Continuous flow conditions

For both physiological and pathological cases, the brain temperature experienced the strongest decrease in the first five to fifteen minutes. Figure 4a shows the average temperature of the entire brain (red) and the mean temperature of the MCA perfusion area (blue) for physiological (dotted lines) and ischemic (solid lines) conditions.

Physiological case: The average temperatures of the entire brain and the MCA perfusion area

showed a strong exponential decrease in the first ten minutes after start of cooling, whereas the decrease in the MCA perfusion area was more pronounced. Subsequently, the decrease slowed in both compartments and the cerebral temperature courses followed the arterial blood temperatures (compare Figure 4b). After 20 min of cooling, the temperature in the MCA perfusion area decreased by 1.8 °C and the mean brain temperature by 0.87 °C. In the further course, the temperature in the MCA perfusion area always remained approximately 0.9 °C below the mean brain temperature. After 60 min of cooling, the temperature in the MCA perfusion area was approximately 34.8 °C and an approximate decrease of 2.25 °C was reached. The systemic temperature decrease was significantly lower, with a value of 0.62 °C after 1 h of cooling.

Ischemic conditions with MCA M1 occlusion: As can also be observed in stroke patients [36, 37], the initial cerebral temperature, especially in the MCA perfusion area, was elevated (≈ 0.35 °C). Compared to physiological conditions, the temperature decreases were markedly lower. Blood cooling for 20 min led to temperature decreases of 0.5 °C and 0.46 °C in the MCA perfusion area and the averaged brain tissue, respectively. For the first 30 min after start of cooling, the temperature in the MCA perfusion area stayed above the mean brain temperature. After 60 min of blood cooling, the complete brain as well as the MCA perfusion area reached a mean temperature of approximately 36.5 °C. The systemic temperature decreased by 0.35 °C compared to initial conditions.

A continuous decrease of the temperature of the systemic body (equal to the PCA blood temperature) and the ACA blood temperature was observed for both the physiological and the pathological case. Due to the negligible collateral flow under physiological conditions, the MCA blood temperature followed the ACA blood temperature. In the ischemic case, only the blood of the ACA experienced a direct cooling effect. The MCA was only perfused via collaterals, which led to a course of blood temperature reflecting the tissue temperature. Concrete values of temperature change (ten minute intervals) are shown in Table 2, while Figure 5 shows frontal cuts of the spatial cerebral temperature for the physiological (top) and pathological (bottom) case in the initial state, as well as after five and 30 min.

Table 2. Temperature decrease of cerebral tissue and arterial blood in °C over time.

	physiological						**MCA M1 occlusion**					
Time in min	**10**	**20**	**30**	**40**	**50**	**60**	**10**	**20**	**30**	**40**	**50**	**60**
$\Delta T_{V_{\mathrm{Sys}}}$	0.09	0.19	0.30	0.41	0.51	0.62	0.05	0.11	0.17	0.23	0.29	0.35
$\Delta T_{V_{\mathrm{Brain}}}$	0.71	0.87	0.99	1.10	1.21	1.31	0.33	0.46	0.55	0.63	0.69	0.76
$\Delta T_{V_{\mathrm{MCA}}}$	1.62	1.80	1.93	2.04	2.15	2.25	0.27	0.50	0.64	0.73	0.81	0.87
$\Delta T_{q_{\mathrm{in,\,MCA}}}$	0.09	0.19	0.30	0.41	0.52	0.62	0.56	0.68	0.76	0.83	0.90	0.96
$\Delta T_{q_{\mathrm{in,\,ACA}}}$	0.09	0.19	0.30	0.41	0.51	0.62	0.05	0.11	0.16	0.23	0.29	0.35

3.2.2. Simulated recanalization

Figure 6 shows the decrease in cerebral temperatures for simulated vessel recanalization. Tdotted and solid lines show the resulting temperatures for a successfuss recanalisation after 10 and 20 min, respectively.

Compared to the resulting cerebral temperatures without simulated vessel recanalization (compare solid lines in Figure 4a), the increase in blood perfusion due to recanalization clearly led to a faster

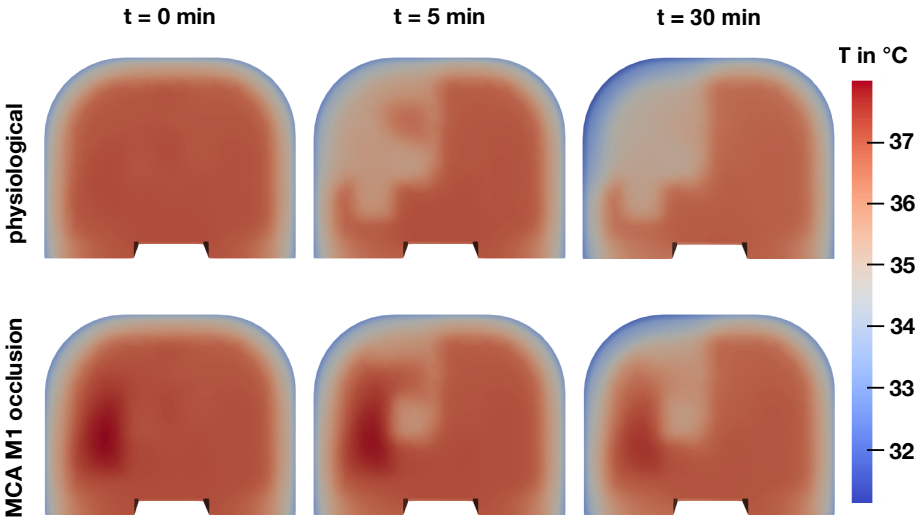

Figure 5. Middle frontal cut of the spatial cerebral temperature distribution for blood cooling in the right CCA (top: physiological, bottom: MCA M1 occlusion).

temperature decrease. After 25 min of cooling, the temperature of the MCA perfusion area was approximately 35.3 °C, if the recanalization was performed after 10 min of cooling. If the recanalization of the MCA M1 occlusion was performed after 20 min, the temperature was about 35.5 °C. Independent of the time of successful recanalization, the temperature decrease of the MCA perfusion area after 1 h of cooling was approximately 2.5 °C. A 2 °C decrease of the MCA perfusion area was reached after 21.6 min, if the recanalization was performed after 10 min of cooling. If the recanalization was performed after 20 min, it took 29.2 min.

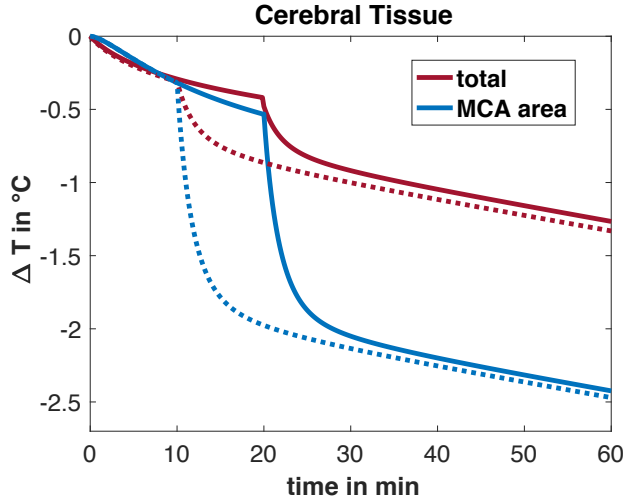

Figure 6. Resulting decrease in cerebral temperatures for simulated successful vessel recanalization. The dotted lines show the resulting temperatures for successful recanalization after 10 min of cooling, whereas the solid lines show the resulting temperatures for a successful recanalization after 20 min.

4. Discussion

In this work, a temperature model of the brain was created with a simplified 3D head geometry. Using a coupled 1D hemodynamics model, spatio-temporal cerebral tissue, arterial blood and mean systemic temperatures were calculated. In several finite element simulations, the resulting temperatures were predicted for the physiological and a pathological (MCA M1 occlusion) state. In this context, selective mild hypothermia by means of an intracarotid blood-cooling catheter was analyzed.

4.1. Model results

4.1.1. Blood flow calculations

Despite the extensive adaptations and extensions of the underlying model by Schwarz et al., our simulated blood flow rates in the main CA showed no major deviations compared to the results of Schwarz et al. In the physiological case, the averaged sum of flow into all terminal segments of the individual main CA should correspond to the given reference flow rate. Our model achieved a mean deviation of about 1.68 %, which is well within this requirement.

For the collateral flow rates, there are no reference values available in the literature. However, it is known that in the physiological case, collateral flow is almost inactive [24]. Our model predicted a negligible average blood flow of 0.00065 $\frac{\text{ml}}{\text{s}}$, which increased approximately to 0.65 $\frac{\text{ml}}{\text{s}}$ during ischemic conditions due to an MCA M1 occlusion.

Konstas et al. [35] determined, using positron emission tomography, an average value of 3.34 $\frac{\text{ml}}{\text{s·kg}}$ for the perfusion rate in the penumbra. Our model showed a perfusion rate of 2.1 $\frac{\text{ml}}{\text{s·kg}}$ for a complete MCA M1 occlusion in the MCA perfusion area. However, the influence of the degree of vessel occlusion and patient-specific collateralization must be taken into account.

4.1.2. Temperature calculation

Therapy for AIS is aiming at a quick establishment of mild local hypothermia in the ischemic brain tissue. Our model predicted a temperature decrease in the MCA perfusion area of approximately 2 °C after 30 min of cooling. However, in the case of an MCA M1 occlusion without recanalization, a maximum cooling of the MCA perfusion area of approximately 0.8 °C was predicted after one hour of cooling. The reason for the lower cooling effect was not only reduced perfusion (corresponding to a reduced ability to dissipate metabolic heat), but also the temperature of the blood flowing into the MCA, which, under ischemic condition, was blood coming from the primary and secondary collaterals. Since the intracarotid cooling catheter cools the blood within the right CCA, only the blood flow from the ACA-MCA collaterals was able to lower the cerebral temperature. Nevertheless, the simulation of vessel recanalization predicted a temperature decrease in the penumbra of approximately 2 °C after 30 min and 2.5 °C after one hour of cooling, which is within target temperature range for neuroprotective effects in hypothermia treatment of AIS [1, 7, 8, 38]. Additionally, in case of a successful recanalization, the cerebral temperature decreased distinctly by about 1.5 °C in the first 5 min after restoration of physiological flow conditions (compare Figure 6). This immediate temperature decrease could mitigate reperfusion injury, since the molecular pathways of reperfusion injury are most prominent in the first 15 min following reperfusion [39].

Nevertheless, the neuroprotective effect would further benefit from an improved cooling perfor-

mance of the catheter. For this, the flow rate of the coolant in the catheter would have to be increased, since an enlargement of the catheter is limited by the artery size. A reduction of the wall thickness of the catheter has hardly any influence on the cooling performance [40]. In addition, the catheter could be insulated against heating of the coolant in the proximal vessels, which was shown to be successful for the administration of cold saline solution [41].

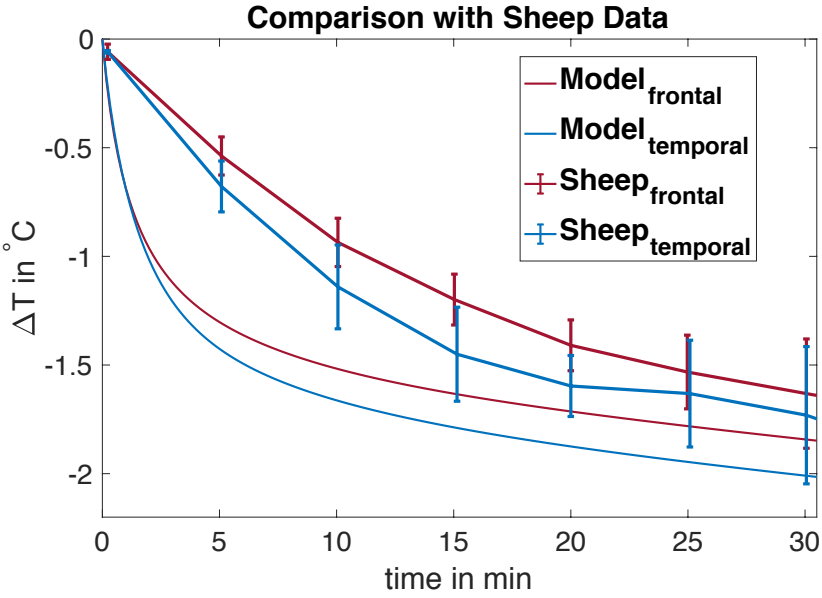

Figure 7. Comparison of predicted cerebral temperatures with measurements in sheep.

Unfortunately, a direct comparison of our results with clinical studies is not possible, as there are no human studies with the new catheter system available yet. However, our predicted temperature curves, agree with first results of animal experiments. In a recent study in nine sheep, the decrease of the animals' cerebral temperature due to blood cooling with the novel cooling catheter system was analyzed. Measuring probes were placed in the frontal and temporal brain cortices and the cooling sheath was located in the CCA. A detailed description of the whole setup can be found in [10]. A comparison between the experimental data and temperature decrease predicted by our model is shown in Figure 7. The model results show a comparable temperature course to the measurements in the animal. In the first 15 min after start of cooling, the measurements do show a milder temperature decrease compared to our results. This could be caused by higher blood flow velocities in the internal carotid artery of sheep [10, 42]. In addition, a direct comparison of the temperature decreases is hardly possible due to the different arterial and cerebral anatomies between human and sheep.

4.2. Limitations

For a more detailed modeling of the main CAs compared to Schwarz et al., an extensive literature research was performed. However, not all needed parameters could be found in literature (compare Section 5). Therefore, some parameters were determined by averaging or by comparison with other comparable arteries. These assumptions could influence the calculated flow and pressure profiles in the arterial network. However, since the terminal resistances of the arterial network were calculated taking into account realistic perfusion rates of GM and WM, the assumptions have no direct influence

on the perfusion rates used for the temperature calculation. In addition, all calculated flows into the CAs well adhere to the defined flow boundary conditions.

For the division of the total brain tissue into GM and WM, the studies of Taki et al. and Ge et al. were used. These studies were conducted independently and showed very similar results. However, the tissue composition of the individual terminal perfusion areas had to be based on empirical assumptions. The local areas are described in detail in the literature, thus plausible assumptions could be made.

The assumed values for the share from the individual main CA in the total brain supply are based on data from Mut et al. [20]. Due to lack of published studies, no further values could be used for comparison. However, the proportions of the volumes correspond to data in anatomy books. The MCA as the largest main CA covers the largest volume, followed by the ACA and the PCA as the smallest main CA.

To calculate reference terminal flow rates, perfusion rates were determined for GM and WM, for which various data can be found in the literature. The values were chosen according to published studies, which include volumetric perfusion rates depending on age and sex, in order to take into account these influencing factors. The resulting ratio of perfusion between GM and WM was approximately 2.2, which is within the range of literature (1.8 to 4) [34]. In addition, the selected perfusion rates resulted in terminal flow rates, that comply with the reference boundary conditions.

Nevertheless, the anatomy of cerebral arteries varies greatly from person to person and our results predict major influence of collateralization on cerebral temperatures. An incomplete circle of Willis, which occurs in about 50 % of the population [43], could further alter the cerebral flow conditions for AIS and lead to altered cooling performance. In this context, a larger simulation study regarding the degree of collateralization and different occlusion scenarios could help to further analyze the respective influences. In addition, our model could be adapted and further expanded to be more detailed. In this work, a simplified 3D brain geometry was used. As a next step a temperature calculation with a realistic MRI-based brain geometry is planned. As a result, the current uncertainties due to assumptions made about the tissue composition of the terminal perfusion areas will be reduced since the use of segmented MRI data ensures a more reliable tissue composition.

5. Conclusions

Our model allows for a realistic temperature calculation within a simplified geometry and can be used to predict the temperature drop by intracarotid blood cooling. In particular, our model can serve to determine an ideal tailored cooling therapy for individual patients, since the successful use of TH depends on a wide variety of factors [38]. In this context, our model can help to solve open questions about the efficiency and optimal use of TTM as an adjunctive neuroprotective therapy to the recanalization therapy of AIS.

Acknowledgements

This study was supported by the German Federal Ministry of Economic Affairs and Energy (ZF4363901AK6).

We acknowledge support by the KIT-Publication Fund of the Karlsruhe Institute of Technology.

Conflict of interest

Giorgio Cattaneo was employed with Adceris GmbH & Co KG until 31.08.2019. All other authors declare no conflict of interest.

References

1. V. D. Worp, H. Bart, E. S. Sena, et al., Hypothermia in animal models of acute ischaemic stroke: a systematic review and meta-analysis, *Brain*, **12** (2007), 3063–3074.
2. H. Chen, M. Chopp, Z. G. Zhang, et al., The Effect of Hypothermia on Transient Middle Cerebral Artery Occlusion in the Rat, *J. Cereb. Blood Flow. Metab.*, **4** (1992), 621–628.
3. Y. H. Hwang, J. S. Jeon, Y. W. Kim, et al., Impact of immediate post-reperfusion cooling on outcome in patients with acute stroke and substantial ischemic changes, *J. NeuroInt. Surg.*, **1** (2017), 21–25.
4. S. Schwab, D. Georgiadis, J. Berrouschot, et al., Feasibility and safety of moderate hypothermia after massive hemispheric infarction, *Stroke*, **32** (2001), 2033–2035.
5. H. B. van der Worp, M. R. Macleod, P. M. W. Bath, et al., EuroHYP-1 investigators, 2014. EuroHYP-1: European multicenter, randomized, phase III clinical trial of therapeutic hypothermia plus best medical treatment vs. best medical treatment alone for acute ischemic stroke, *Int. J. Stroke*, **9** (2014), 642–645.
6. T. C. Wu and J. C. Grotta, Hypothermia for acute ischaemic stroke, *Lancet Neurol.*, **3** (2013), 275–284.
7. C. Wu, W. Zhao, H. An, et al., Safety, feasibility, and potential efficacy of intraarterial selective cooling infusion for stroke patients treated with mechanical thrombectomy. *J. Cereb. Blood Flow. Metab.*, **12** (2018), 2251–2260.
8. S. S. Song and P. D. Lyden, Overview of Therapeutic Hypothermia, *Curr. Treat Options Neurol.*, **6** (2012), 541–548.
9. G. Cattaneo, M. Schumacher, J. Wolfertz, et al., Open access combined selective cerebral hypothermia and mechanical artery recanalization in acute ischemic stroke: In vitro study of cooling performance, *Am. J. Neuroradiol.* **11** (2015), 2114–2120.
10. G. Cattaneo, M. Schumacher, C. Maurer, et al., Endovascular Cooling Catheter for Selective Brain Hypothermia: An Animal Feasibility Study of Cooling Performance, *Am. J. Neuroradiol.*, **5** (2016), 885–891.
11. A. P. Avolio, Multi-branched model of the human arterial system, *Med. Biol. Eng. Comput.*, **6** (1980), 709–718.
12. M. Schwarz, *Modellbasierte Operationsplanung und Überwachung hypothermer Patienten*, KIT Scientific Publishing, 2009.
13. M. Schwarz, M. W. Krueger, H. J. Busch, et al., Model-Based Assessment of Tissue Perfusion and Temperature in Deep Hypothermic Patients, *IEEE Transact. Biomed. Eng.*, **7** (2010), 1577–1686.
14. F. Umansky, S. M. Juarez, M. Dujovny, et al., Microsurgical anatomy of the proximal segments of the middle cerebral artery, *J. Neurosurg.*, **3** (1984), 458–467.

15. L. M. Parkes, W. Rashid, D. T. Chard, et al. Normal cerebral perfusion measurements using arterial spin labeling: Reproducibility, stability, and age and gender effects, *Magnet. Reson. Med.*, **4** (2004), 736–743.

16. R. Fahrig, H. Nikolov, A. J. Fox, et al., A threedimensional cardiovascular flow phantom, *Med. Phys.*, **8** (1999), 1589–1599.

17. J. S. Allen, H. Damasio and T. J. Grabowski, Normal neuroanatomical variation in the human brain: an MRI-volumetric study, *Am. J. Phys. Anthropol.*, **4** (2002), 341–358.

18. Y. Ge, R. I. Grossman, J. S. Babb, et al., Age-related total gray matter and white matter changes in normal adult brain, Part II: Quantitative magnetization transfer ratio histogram analysis, *Am. J. Neuroradiol.*, **8** (2002), 1334–1341.

19. Y. Taki, B. Thyreau, S. Kinomura, et al., Correlations among brain gray matter volumes, age, gender, and hemisphere in healthy individuals, *PLOS ONE*, **7** (2011), e22734.

20. F. Mut, S. Wright, G. A. Ascoli, et al., Morphometric, geographic, and territorial characterization of brain arterial trees, *Int. J. Numer. Method Biomed. Eng.* , **7** (2014), 755–766.

21. J. Waschke and F. P. Sobotta, *Atlas der Anatomie des Menschen: Kopf, Hals und Neuroanatomie*. Urban und Fischer Verlag, 2010.

22. W. C. Wu, S. C. Lin, K. L. Wang, et al., Measurement of cerebral white matter perfusion using pseudocontinuous arterial spin labeling 3t magnetic resonance imaging - an experimental and theoretical investigation of feasibility, *PLoS ONE*, 2013.

23. K. Zilles and B. N. Tillmann, *Anatomie* Springer Verlag, 2010.

24. N. Tariq and R. Khatri, Leptomeningeal collaterals in acute ischemic stroke, *J. Vasc. Interv. Neurol.*, **1** (2008), 91–95.

25. D. S. Liebeskind, Collateral circulation, *Stroke*, **8** (2003), 2279–2284.

26. H. M. Vander Eecken and R. D. Adams, The anatomy and functional significance of the meningeal arterial anastomoses of the human brain, *J. Neuropathol. Exper. neurol.*, **12** (1953), 132–157.

27. A. Frydrychowski, A. Szarmach, B. Czaplewski, et al., Subarachnoid space: New tricks by an old dog. *PloS one*, **7** (2012), 37529.

28. A. Bashkatov, E. Genina, Y. P. Sinichkin, et al., Glucose and mannitol diffusion in human dura mater, *Biophys. J.*, **85** (2003), 3310–3318.

29. H. Li, J. Ruan, Z. Xie, et al., Investigation of the critical geometric characteristics of living human skulls utilising medical image analysis techniques, *Int. J. Veh. Saf.*,**2** (2007), 345–367.

30. H. Hori, G. Moretti, A. Rebora, et al., The thickness of human scalp: normal and bald, *J. Invest. Dermatol.*, **6** (1972), 396–369.

31. M. Geerligs, *Skin layer mechanics*, PhD thesis, Department of Biomedical Engineering, TU Eindhoven, Eindhoven 2010.

32. H. H. Pennes, Analysis of Tissue and Arterial Blood Temperatures in the Resting Human Forearm, *J. Appl. Physiol.*, **1** (1948), 5–34.

33. B. Pliskov, K. Mitra and M. Kaya, Simulation of scalp cooling by external devices for prevention of chemotherapy-induced alopecia, *J. Therm. Biol.*, **56** (2016), 199–205.

34. P. Hasgall, F. Di Gennaro, C. Baumgartner, et al., IT'IS Database for thermal and electromagnetic parameters of biological tissues, vol. 4.0, May 2018. Available from: itis.swiss/database

35. A.-A. Konstas, M. A. Neimark, A. F. Laine, et al., A theoretical model of selective cooling using intracarotid cold saline infusion in the human brain, *J. Appl. Physiol.*, **4** (2007), 1329–1340.

36. L. Mcilvoy, Comparison of brain temperature to core temperature: a review of the literature. *J. Neurosci. Nurs.*, **1** (2004), 23–31.

37. B. Karaszewski, J. M. Wardlaw, I. Marshall, et al., Measurement of brain temperature with magnetic resonance spectroscopy in acute ischemic stroke., *Ann. Neurol.*, **4** (2006), 438–446.

38. T. C. Jackson and P. M. Kochanek. A New Vision for Therapeutic Hypothermia in the Era of Targeted Temperature Management: A Speculative Synthesis. *Ther. Hypothermia Tem. Manag.*, **1** (2019), 13–47.

39. J. N. Stankowski and R. Gupta, Therapeutic targets for neuroprotection in acute ischemic stroke: lost in translation?, *Antioxid. Redox Signal.*, **10** (2011), 1841–1851.

40. J. Wolfertz, S. Meckel, A. Guber, et al., Mathematical, numerical and in-vitro investigation of cooling performance of an intra-carotid catheter for selective brain hypothermia, *Curr. Direct. Biomed. Eng.*, **1** (2015), 390–394.

41. J. Caroff, R. M. King, J. E. Mitchell, et al., Focal cooling of brain parenchyma in a transient large vessel occlusion model: proof-of-concept, *J. NeuroInt. Surg.*, (2019), 1–6.

42. Y. Lutz, A. Loewe, S. Meckel, et al., Combined Local Hypothermia and Recanalization Therapy for Acute Ischemic Stroke: Estimation of Brain and Systemic Temperature Using an Energetic Numerical Model, *Thermal Biol.*, **84** (2019), 316–322.

43. H. Lippert and R. Papst, Arterial variations in man: classification and frequency, *J.F. Bergmann-Verlag Mnchen*, 1985.

44. K. Cilliers, Anatomy of the middle cerebral artery: Cortical branches, branching pattern and anomalies, *Trukish Neurosurg.*, **5**(2017), 671–681.

45. M. A. Stefani, F. L. Schneider, A. C. H. Marrone, et al., Anatomic variations of anterior cerebral artery cortical branches, *Clin. Anat.*, **4** (2000), 231–236.

46. K. Cilliers and B. Page, Detailed description of the anterior cerebral artery anomalies observed in a cadaver population, *Ann. Anatomy-Anat. Anz.*, **208** (2016),1–8.

47. A. A. Zeal and A. L. Rhoton Jr., Microsurgical anatomy of the posterior cerebral artery, *J. Neurosurg.*, **4** (1978), 534–559.

48. M. Pham and M. Bendszus, Facing time in ischemic stroke: an alternative hypothesis for collateral failure, *Clin. Neuroradiol.*, **2** (2016), 141–151.

Supplementary material

1. Modeling the cerebral arterial network

As mentioned in Section 2.1, a 1D transmission-line-approach was used for modeling the cerebral arterial blood flow. The blood is regarded as an imcompressible Newtonian fluid. The use of linearized

and one-dimensional Navier-Stokes equations leads to two relations between pressure p and flow q:

$$-\frac{\partial p}{\partial z} = \frac{\rho}{\pi r^2} \cdot \frac{\partial q}{\partial t} + \frac{8\eta}{\pi r^4} \cdot q, \tag{5.1}$$

$$-\frac{\partial q}{\partial z} = \frac{3\pi r^3}{2Ed} \cdot \frac{\partial p}{\partial t}. \tag{5.2}$$

Here, η is the dynamic blood viscosity ($= 2.3 \cdot 10^{-3}\ \frac{kg}{ms}$), ρ the blood density ($= 1020\ \frac{kg}{m^3}$), r the vessel inner radius, E Young's modulus and d the wall thickness of the respective arterial segment. Replacing the pressure by the voltage and the blood flow by the electric current and making use of the following coefficients:

$$R = \frac{8\eta\Delta z}{\pi r^4}, \quad L = \frac{\rho\Delta z}{\pi r^2}, \quad C = \frac{3\pi r^3 \Delta z}{2Ed}, \tag{5.3}$$

leads to an electrical analogon of hemodynamics. There, Δz represents the unit length. R reflects the respective flow resistance, L the inertance and C the compliance in the respective arterial segment. An arterial segment with a length Δz is represented by a discrete *RLC* quadripole. For discretization four different possibilities exist (standard, inverse, π and T). For the standard quadripole, the following equations can be established:

$$\frac{dp_{\text{out}}}{dt} = \frac{1}{C} \cdot (q_{\text{in}} - q_{\text{out}}), \tag{5.4}$$

$$\frac{dq_{\text{in}}}{dt} = -\frac{R}{L} \cdot q_{\text{in}} + \frac{1}{L} \cdot (p_{\text{in}} - p_{\text{out}}). \tag{5.5}$$

To solve the equations, the input pressure p_{in} and the output flow q_{out} have to be given as input values.

Applying Kirchhoff's first law for electrical circuits, it is possible to model series and parallel connections between several segments, whereas the influence of the angle between branching arteries is neglected. Furthermore, long arteries can be replaced by series of standard quadripoles and collateral connections can be modeled with parallel type T quadripoles. [11, 12, 13]

1.1. Model of the Cerebral Arterial Tree

In this work, an extended model of the cerebral structure is required to investigate the impact of collateral circulation on cerebral temperature. Therefore, the three main cerebral arteries were modeled in more detail and ipsilateral collaterals were integrated into the model. However, in literature the arteries outer diameters are specified, generally. To determine the required inner radius r_{inner} and the wall thickness d of the respective vessels, a translation was performed. Analyzing the values given in Avolio's model [11], a factor between inner and outer radius r_{outer} was determined:

$$r_{inner} = 0.78 \cdot r_{outer}, \quad d = 0.22 \cdot r_{outer} \tag{5.6}$$

As the literature, to our knowledge, does not provide information on Young's modulus for all required arteries, we took the missing data from arteries of similar dimensions from Avolio's model.

All parameters of the vessels required by the transmission-line-approach of our hemodynamics model are listed in the following tables:

Table 3. Added arterial segments of the cerebral circulation. Values marked with * were calculated as a mean value of the MCA cortical branches, due to a lack of precise information for the ACA and PCA cortical branches.

Segment	Artery description	Length (cm)	Radius (cm)	Wall thickness (cm)	Source
139	M1 segment (right)	0.75	0.117	0.033	[14]
140	M1 segment (r)	0.59	0.117	0.033	[14]
141	M1 segment (r)	0.16	0.117	0.033	[14]
142	M1 segment (left)	0.74	0.117	0.033	[14]
143	M1 segment (l)	0.83	0.117	0.033	[14]
144	M2 superior (r)	0.45	0.0819	0.0231	[14]
145	M2 superior (r)	0.78	0.0819	0.0231	[14]
146	M2 superior (r)	0.03	0.0819	0.0231	[14]
147	M2 superior (l)	0.32	0.078	0.022	[14]
148	M2 superior (l)	0.92	0.078	0.022	[14]
149	M2 superior (l)	0.27	0.078	0.022	[14]
150	M2 inferior (r)	0.84	0.0897	0.0253	[14]
151	M2 inferior (r)	0.75	0.0897	0.0253	[14]
152	M2 inferior (r)	0.20	0.0897	0.0253	[14]
153	M2 inferior (r)	0.12	0.0897	0.0253	[14]
154	M2 inferior (r)	0.16	0.0897	0.0253	[14]
155	M2 inferior (l)	0.26	0.078	0.022	[14]
156	M2 inferior (l)	1.00	0.078	0.022	[14]
157	M2 inferior (l)	0.29	0.078	0.022	[14]
158	M2 inferior (l)	0.08	0.078	0.022	[14]
159	M2 inferior (l)	0.09	0.078	0.022	[14]
160	M2 inferior (l)	0.01	0.078	0.022	[14]
161	orbitofrontal (r)	1.83	0.0429	0.0121	[44]
162	oribtofrontal (l)	1.89	0.039	0.011	[44]
163	precentral (r)	2.34	0.0468	0.0132	[44]
164	precentral (l)	2.26	0.0546	0.0154	[44]
165	central (r)	2.31	0.0507	0.0143	[44]
166	central (l)	1.99	0.0546	0.0154	[44]
167	anterior parietal (r)	3.42	0.0468	0.0132	[44]
168	anterior parietal (l)	3.51	0.0468	0.0132	[44]
169	posterior parietal (r)	4.5	0.0507	0.0143	[44]
170	posterior parietal (l)	4.95	0.0585	0.0165	[44]
171	angular (r)	5.98	0.0585	0.0165	[44]
172	angular (l)	6.1	0.0585	0.0165	[44]
173	temporopolar (r)	1.76	0.0312	0.0088	[44]
174	temporopolar (l)	1.77	0.0351	0.0099	[44]
175	anterior temporal (r)	2.58	0.0468	0.0132	[44]

Segment	Artery description	Length (cm)	Radius (cm)	Wall thickness (cm)	Source
176	anterior temporal (l)	2.09	0.0468	0.0132	[44]
177	middle temporal (r)	3.15	0.0507	0.0143	[44]
178	middle temporal (l)	2.66	0.0468	0.0132	[44]
179	posterior temporal (r)	4.82	0.0546	0.0154	[44]
180	posterior temporal (l)	4.61	0.0507	0.0143	[44]
181	A2 segment (r & l)	0.77	0.0897	0.0253	[45]
182	A2 segment (r & l)	1.39	0.0897	0.0253	[45]
183	A2 segment (r & l)	0.78	0.0897	0.0253	[45]
184	A3 segment (r & l)	3.63	0.0819	0.0231	[45]
185	A4 segment (r & l)	2.54	0.0624	0.0176	[45]
186	A5 segment (r & l)	1.1	0.0429	0.0121	[45]
187	CmA (r & l)	1.19	0.0702	0.0198	[45]
188	CmA (r & l)	1.55	0.0702	0.0198	[45]
189	CmA (r & l)	1.35	0.0702	0.0198	[45]
190	CmA (r & l)	1.45	0.0702	0.0198	[45]
191	infra-orbital (r & l)	3.216*	0.0351	0.0099	[46]
192	frontopolar (r & l)	3.216*	0.0351	0.0099	[46]
193	anterior internal frontal (r & l)	3.216*	0.0429	0.0121	[46]
194	middle internal frontal (r & l)	3.216*	0.0468	0.0132	[46]
195	posterior internal frontal (r & l)	3.216*	0.0507	0.0143	[46]
196	paracentral (r & l)	3.216*	0.0507	0.0143	[46]
197	superior internal parietal (r & l)	3.216*	0.0468	0.0132	[46]
198	inferior internal parietal (r & l)	3.216*	0.039	0.011	[46]
201	P2 segment (r & l)	1.44	0.1131	0.0139	[47]
202	P2 segment (r & l)	0.16	0.1131	0.0139	[47]
203	P2 segment (r & l)	0.34	0.1131	0.0139	[47]
204	P2 segment (r & l)	0.30	0.1131	0.0139	[47]
205	P2 segment (r & l)	0.23	0.1131	0.0139	[47]
206	P2 segment (r & l)	0.37	0.1131	0.0139	[47]
207	P2 segment (r & l)	1.06	0.1131	0.0139	[47]
208	hippocampal (r & l)	3.216*	0.0312	0.0088	[47]
209	anterior temporal (PCA) (r & l)	3.216*	0.0507	0.0143	[47]
210	middle temporal (MCA) (r & l)	3.216*	0.0468	0.0132	[47]
211	common temporal (r & l)	3.216*	0.0741	0.0209	[47]
212	parieto-occipital (r & l)	3.216*	0.0624	0.0176	[47]
213	posterior temporal (PCA) (r & l)	3.216*	0.0624	0.0176	[47]
214	calcarine (r & l)	3.216*	0.0546	0.0154	[47]

Table 4. Added ipsilateral collaterals. The inner radii of the collaterals were multiplied by the factor 1.5 to take into account the presence of further smaller collaterals. The respective lengths were calculated using data of Pham et al. [48].

Collateral	Length (cm)	Radius (cm)	Wall thickness (cm)	Source
ACA–MCA r / l	3.934*	0.0143	0.004	[26]
ACA–MCA r / l	3.734*	0.0139	0.0039	[26]
ACA–MCA r / l	3.58*	0.0143	0.004	[26]
PCA–MCA r / l	3.75*	0.0112	0.0031	[26]
PCA–MCA r / l	3.75*	0.0197	0.0055	[26]
PCA–MCA r / l	3.75*	0.0129	0.0036	[26]
PCA–ACA r / l	3.75*	0.0091	0.0026	[26]

AIMS Press